

Improving the pseudo-randomness properties of chaotic maps using deep-zoom

Jeaneth Machicao¹, Odemir Martinez Bruno¹

¹São Carlos Institute of Physics, University of São Paulo, São Carlos - SP, PO Box 369, 13560-970, Brazil.
Scientific Computing Group - <http://scg.ifsc.usp.br>

Abstract

A generalized method to compound new orbits of an underlying chaotic map, which endeavors for the k -right decimals of the original orbit is proposed. The method provides an approach to examine discrete-time chaotic maps into a “deep zoom” manner by means of their k -right digits of precision. Interesting phenomena have been identified. A rapid randomization has been observed, i.e. the chaotic patterns tend to become indistinguishable, when comparing with the original orbits of the underlying chaotic map. It was observed by several graphical analysis (i.e. time-evolution, bifurcation diagram, Lyapunov exponent, Poincaré diagram and frequency distribution). Moreover, taking advantage of this randomization enhancing, we proposed a pseudo-random number generator (PRNG) based on the k -logistic map. The pseudo-randomness quality of the proposed PRNG passes successfully by using both statistical tests, i.e. Diehard and NIST suits, being comparable to traditional PRNGs such as the Mersenne Twister. The results suggest that simple maps such as the logistic map can be considered as good PRNG methods.

1 Introduction

Random numbers have a significant role in diverse fields and in many demanding applications [1, 2, 3] ranging from statistical mechanics, decision theory, calculus, games and gambling industry; to more crucial pursuits such as cryptography and computer simulations. Consequently, in recent years, huge attention was put on generating such numbers.

In fact, methods for generating random numbers can be broadly divided into two main approaches: true random number generator (TRNG) and pseudo-random number generator. On one hand, TRNGs rely on the physical sources such as throwing dice or flipping coin, to more sophisticated processes such as radius material decay [4, 5], thermal noise in resistors [6], atmospheric noise [7, 8], lava lamps [9] and quantum physics [10, 11]. However, there are certain inconveniences in terms of its implementation, including additional special equipment and circuitry (often require either cooling or high voltages), limited speed, restricted rates of production, e.g 16 Mbps [12], and degradation of the statistical properties when implemented in hardware and software level [13].

On the other hand, PRNGs can generate pseudo-random numbers depending on deterministic sources by inputting an initial seed to a given algorithm, such as the linear congruential generator (LCG) [1, 2], the Mersenne Twister [14], nonlinear LCG [15], linear feedback shift registers (LFSR) [16], among others numerical algorithms. The main advantages of PRNGs rely on its determinism (repeatability of the pseudo-random sequences), which for certain purposes is a desirable characteristic in special considering cryptography and one-way function (hashing algorithms). Although PRNGs are periodic, due to the technological advances, most construction presents large periodicity that can be ignored for most practical purposes. Moreover, PRNGs are efficient to produce many numbers in a short time, have inexpensive requirements and are easy to implement. Many of these classical PRNGs, such as the old fashion RANDU, have already been cryptanalyzed [17, 18]. Therefore, much effort was put to develop alternative PRNG proposals to fill the need for “good” sources of pseudo-randomness.

During the last 30 years, many scientists noticed an interesting relationship between chaos and pseudo-randomness [19, 20, 21, 22, 23]. Since chaos meets desirable properties for cryptographic and cryptanalysis [24] purposes. The distinct properties of chaos, such as diffusion and confusion can, in principle, assure pseudo-random numbers of high-quality, mainly because of the sensitivity to initial conditions, ergodicity, mixing properties, complex numerical patterns, relatively simple equation and its determinism [23, 25, 20, 26]. Therefore, huge progresses have been reported, for instances chaos-based PRNGs were proposed using chaotic systems [27, 28, 29, 30, 31, 32, 33, 34],

cellular automata [35, 36, 37], quantum chaotic maps [38, 39, 40] and even mixing the physical chaotic sources, e.g. chaotic semiconductor lasers [41, 42].

Recalling to the first chaos-based cryptosystem appeared at late 90s [21]. Baptista explored the pseudo-randomness advantages from the logistic map as PRNG, i.e. generating sequences of bits to later be used by the cipher [21]. However, the relationship between chaos and cryptography has been questioned, criticized and discouraged after Baptista’s cryptosystem fault [43, 44]. These researchers exhibited certain issues with the pseudo-randomness properties of the logistic map such as (i) non-uniform probability distribution (U pattern), where is expected a plateau distribution [43]; ii) dependency on the control parameter, consequently lead to periodic windows [43]; iii) sufficiently large sample of ciphertext may allow to estimate the parameter [43]; and (v) trajectories of short cycle length where is expected longer periodicity depending on machine limitations [44]; (vi) degradation of digital chaotic systems issue [45].

Though, the true potential from chaos is being dismissed since many researchers have been neglected the fact that chaos analytically rely on the infinitesimal depth of precision digits from their orbit points. For instance, taking into account the well-known Mandelbrot set [46], when it is displayed into a computer screen, it reveals interesting but quite limited patterns. Nevertheless, when this single pattern is magnified repeatedly, a huge number of complex patterns can be distinguished, and, effectively, is in these magnification views where legitimate chaos occurs. Thus, higher computing precision are required in order to explore into the deep-zoom level of a chaotic system and consequently to explore the pseudo-randomness properties of chaotic systems.

In this paper, we proposed an approach to improve the pseudo-randomness properties of a PRNG based on chaotic maps. The main idea is to perform a deep-zoom exploration of the chaotic orbits in order to generate more chaotic orbits. Here, we focus into the logistic map, as such map is a very familiar and well understood in chaos theory. Specifically, each x^t value from an orbit was explored by considering the k -right digits of precision, which we coined as k -logistic map to the orbits derived from the underlying orbit $k = 0$. Furthermore, the PRNG based on the k -logistic map was subjected to statistical randomness test in order to show the strong properties from the chaotic systems.

In the remainder of this paper, Section 2 presents a short background regarding round-off errors and dynamical degradation in chaotic systems. Section 3 outlines the mathematical definitions of the proposed approach, to later introduce the k -logistic map. We divide the experiments into two parts. Firstly, Section 4 shows the overall dynamic properties of the k -logistic map. Secondly, Section 5 presents the pseudo-randomness analysis by means of the DIEHARD [47] and NIST [48] suits, and finally a comparison analysis is performed with other chaotic map and classical PRNGs. Section 7 ends with discussions about the results, and conclusions are drawn in Section 8.

2 Preliminaries

2.1 Influence of round-off errors and dynamical degradation of chaotic systems

The pillar of the chaos theory states that the smallest change in the initial conditions of a chaotic dynamical system will eventually lead to an exponential rate of separation from the original orbit [49]. Consequently, the digits of precision are one important issue for numerical studies of chaotic systems. For instances, consider the logistic map given by Eq. 1

$$x_{t+1} = f(x_t) = \mu x_t(1 - x_t), \tag{1}$$

where $\mu \in [0, 4]$, $x \in [0, 1]$ and t the discrete time step [49]; and consider an orbit of the logistic map constituted analytically with parameter $\mu = 4$. One can observe how the number of digits of precision exponentially expands while iterates,

$$\begin{aligned} x_0 &= 0.4, \\ x_1 &= 0.96, \\ x_2 &= 0.1536, \\ x_3 &= 0.52002816, \\ x_4 &= 0.9983954912280576, \\ x_5 &= 0.00640773729417263956570612432896, \\ x_6 &= 0.0254667127877660346612116173277063894732481849833090031588212736 \end{aligned}$$

The floating-point arithmetic is a very important topic in computer science. In many computations, the precision of the results are progressively degraded as a result of “round-off error”. A typical case of this issue is exemplified in Table 1.

Table 1: Round-off applied to three orbits (columns) generated by the logistic map with same initial conditions and parameters using 4, . . . , 6 computing digits of precision.

t	computing digits of precision		
	4	5	6
0	0.4782	0.47820	0.478200
1	0.9981	0.99810	0.998099
2	0.0076	0.00759	0.007590
3	0.0302	0.03013	0.030130
\vdots		\vdots	
100	0.3997	0.68170	0.246600

In this experiment it was used round-off on the 4, . . . , 6-th computing digits of precision, while computing $t = 100$ time steps on the logistic map using the same initial condition and parameters $\mu = 4$. One can observe that, in the long-term x_{100} , each of the orbits have departed away from the others orbits.

On the other hand, the so called dynamical degradation [45] occurs when a chaotic system is realized in finite computing precision with L -bit finite precision and fixed-point arithmetic is adopted. Thus, the initial conditions, control parameters and the orbit values are formulated as $a/2^L$ with $a = 0 \sim 2^L - 1$, and therefore there are only 2^L digital values to represent the chaotic orbits, so the period length of the orbits will not be larger than 2^L [50]. For this reason, it is not feasible to compute the orbit with the same precision than obtained analytically. However, one way to circumvent this two issue by using higher computing precision. Thus, in this manuscript we used the Afloat¹ library, which is a high performance arbitrary precision arithmetic, which was employed though all the experiments presented here.

2.2 Number of iterations to reach chaos regime

The number of iterations needed for two initial orbits, slightly separated, get considerably apart is also related to the round-off issue. For instance, we estimated the number of iterations τ needed to achieve $|f^\tau(x) - f^\tau(x')| > 10^{-1}$ when given an initial condition x_0 and its perturbed part $x' = x_0 + \epsilon$ separated apart by a distance $\epsilon = 10^{-d}$ and the parameter $\mu = 4$, which is known to lead to chaotic regime. Here, the exponent d represents the number of digits of precision $d = \lfloor \log |x_0 - x'| \rfloor$.

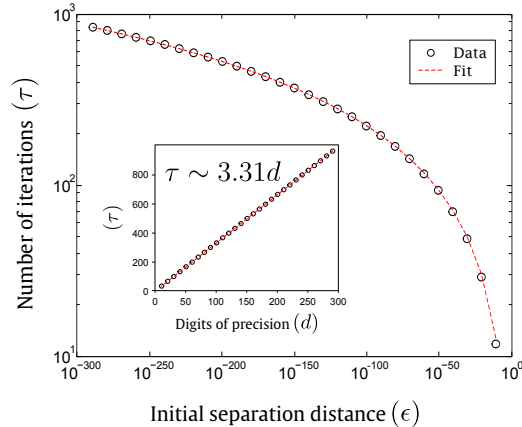


Figure 1: Log-log plot of the number of iterations τ needed to achieve $f^\tau(x) - f^\tau(x') > 0.1$ when two orbits are separated apart at a distance ϵ (solid line). The inner plot shows the same results where the initial distance is shown in terms of the digits of precision d . The function $f(x)$ was related to the logistic map (Eq. 1). The goodness statistic of the fit curve $\tau \sim 3.311d$ (dotted red line) are $R^2 = 0.99$ and $\chi^2 = 56.2$.

Fig. 1 depicts a log-log plot of data obtained from several random initial conditions and its separation distances

¹<http://www.apfloat.org/>

$\epsilon = \{10^{-10}, 10^{-20}, \dots, 10^{-290}\}$, while the inner plot shows the same results but the initial separation distance is configured in terms of the digits of precision $d = \{10, 20, \dots, 290\}$. Regarding this plot, we found a linear approximation $\tau \sim 3.311d$, which suggests that the number of iterations τ needed for two initial orbits, slightly separated, get far apart should be at least three times the number of d digits of precision been used.

3 k-right digits of the Logistic map

A one-dimensional discrete dynamical system (DDS) can be described by a recurrence equation $x_{t+1} = f(\mu, x_t)$ such that $f : M \mapsto M$ is a map where x_t at a particular time $t \in \mathbb{N}_0$ represents all the information characterizing a system given an initial state x_0 in the phase-space $M \subset \mathbb{R}$, which depends on the control parameter $U \subset \mathbb{R}$. Therefore, an orbit $\mathcal{O}(\mu, x_0) = \{x_0, x_1, \dots, x_t\}$ is a collection of points related by the evolution function of the DDS. For instance, the logistic map (Eq. 1) is formalized as $f(\mu, x_{t+1}) = \mu x_t(1 - x_t)$ such that $x_t \in M = [0, 1]$ and $\mu \in U = [0, 4]$.

Definition 1. Let $\mathcal{O}^k(\mu, x_0) = \{x_0^k, x_1^k, \dots, x_t^k\}$ the resulting orbit derived from an already observed orbit $\mathcal{O}(\mu, x_0)$, or simply $\mathcal{O}^{k=0}$. The new value x_t^k is created by retaining k -decimals to the right of the decimal separator corresponding to a given point $x_t \in \mathcal{O}^{k=0}$. Thus, Eq. 2 is the generalized approach to analyze the k -right digits of precision of a one-dimensional DDS

$$x_t^k = \phi_{k,L}(x_t) = \frac{\lfloor x_t 10^{k+L} \rfloor}{10^L} - \lfloor x_t 10^k \rfloor, \quad (2)$$

where L is the length of digits of precision of the new point x_t^k , and $\lfloor \cdot \rfloor$ stands for the floor function.

Clearly, some constraints must be taken into account.

- $k \leq L$;
- $k + L \leq \text{lenght}\{x_t^{k=0}\} - 2$, otherwise the resulting value is padded with zeros;
- the transient time, i.e the number of iterations before the systems settle down, must be at least three times the number of digits of precision been used.

Moreover, the numbers of digits precision L should not be confused with the computing precision of the underlying configuration, which in practice, should use higher precision as possible.

Definition 2. The resulting orbit $\mathcal{O}^k(\mu, x_0)$, hereafter k -logistic map, is a straightforward function to generate orbits derived from an underlying orbit $\mathcal{O}^{k=0}(\mu, x_0)$, such that the resulting orbit still maintains its parameters $\mu \in [0, 4]$, x_t^k in the unitary interval $[0, 1]$. For example, given two points $x_t = 0.268932$ and $x_{t+1} = 0.786430317504$ of an orbit $\mathcal{O}^{k=0}$. One steps rightward the first digits to the right, therefore, e.g $\phi_{k=1,L=3}(x_t) = 0.689$ while $\phi_{k=1,L=3}(x_{t+1}) = 0.864$. Another example, $\phi_{k=3,L=4}(x_t) = 0.9320$ while $\phi_{k=3,L=4}(x_{t+1}) = 0.4303$, and so on.

Definition 3. Furthermore, some formal definitions of Lyapunov exponent for one-dimensional maps are recalled below. Typically, the LE can be assessed analytically by using Eq. 3.

$$\lambda(\mu, x_0) = \lim_{T \rightarrow \infty} \frac{1}{T} \sum_{t=0}^{T-1} \ln |f(\mu, x)'(x_t)|. \quad (3)$$

Therefore, we can approximate the LE for the new constituting orbit \mathcal{O}^k by using Wolf's method to seek Lyapunov exponents in times series [51]. Thus, given two orbits in the phase space with initial separation $d_0 = |\phi_k(f(x_0 + \epsilon)) - \phi_k(f(x_0))|$ diverge at a rate given by $\epsilon e^{t\lambda(x_0)}$ for long term T . The LE for one-dimensional maps $\lambda(\mu, x_t^k)$, such as the k -logistic map is given by Eq. 4, as follows

$$\lambda(\mu, x_t^k) = \frac{1}{T\Delta t} \sum_{t=1}^T \ln \left(\frac{d_t}{d_0} \right), \quad (4)$$

where Δt is the number of time steps in the fiduciary trajectory, and T is the number of times through the loop inside Eq. 4, and $d_t = |\phi_k(f^{\Delta t}(x_0 + \epsilon)) - \phi_k(f^{\Delta t}(x_0))|$. For more suitable numerical computations, we discretize the time into interval of length Δt , such that the total number of time-steps is $T\Delta t$.

4 Analysis of k-logistic map

In this section we analyzed the overall dynamic properties of the orbits generated by the k -logistic map (Eq. 2) by means of several plots including time-evolution (Section 4.1), bifurcation diagram and skeleton bifurcation diagram (Section 4.2), statistical analysis with Lyapunov exponents (Section 4.3), phase diagrams (Section 4.4) and frequency distribution plots (Section 4.5). Moreover, for all of these experiments, we employed 500 digits of precision by using the Apfloat library, so that we can expand the to generate new values as k increases. Additionally, hereinafter the terms k_i and $k = i$ are used indistinctly.

4.1 Time-evolution

Fig. 2 depicts the time-evolution of the k -logistic map corresponding to the orbits from k_0 (original) to k_4 during $t = 100$ iterations. Here, we used specific parameters $\mu = 4$, $\mu = 3.57$ and $\mu = 2.85$ that lead to the three well-known Lyapunov stability behaviors, i.e. chaotic, periodic and stable respectively. The plots in Fig. 2-a) shown two nearby close orbits with initial conditions x_0 and x'_t , using the parameter $\mu = 4$ that leads to chaotic regime. One can observe that the transient time before both curves diverge is reduced approximately from 31 (k_0) to 17 (k_4). Fig. 2-b) depicts the plots on the periodic regime, here we can notice a periodic pattern (k_0) that gets repeated almost 24 times across the $t = 100$ iterations, while the periodic sequence on k_1 is repeated 6 times, in k_2 is repeated almost 2 times, in k_3 and k_4 the period length is bigger than $t = 100$ iterations and cannot be observed in this plot. Finally, observing at the steady regime in Fig. 2-c), the number of iterations before reaching a convergence to a fixed point is increased successively around 11 (k_0) to 71 (k_4).

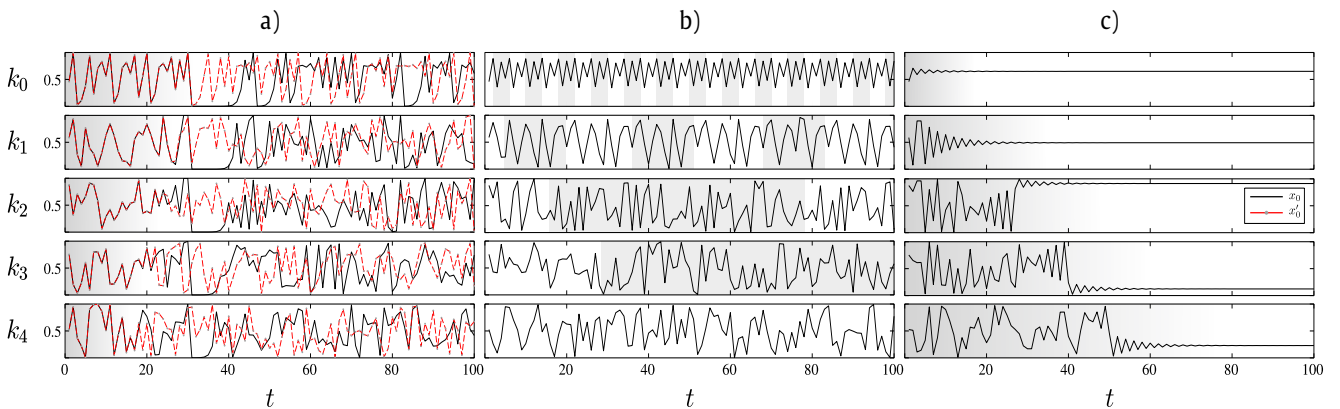


Figure 2: Time-evolution of two orbits with close initial conditions $x_0 = 0.4587525281$ (solid line) and $x'_0 = 0.4587525282$ (dotted line) using the parameters (a) $\mu = 4.0$ (b) $\mu = 3.57$ and (c) $\mu = 2.85$, over $t = 100$ iterations, considering from $k = 0$ to $k = 4$ decimal digits (top to down). The light gray watermark represents a) the number of iterations for the two orbits diverge from each other, b) the length of the periods and c) the number of iterations until the orbit converges.

Regarding these plots, we observed both stretching and shrinking course of the curves depending on the control parameter μ while k is increased. Notwithstanding, the corresponding LE stability of the original curve (k_0) is maintained as k increases, for instances, in the chaotic region there, the transient time is decreased; in the periodic region, the cycles get bigger lengths, and the number of iteration on the stable regime before the convergence is increased.

4.2 Bifurcation Diagram

Fig. 3-a), from top to down, shows the well-known bifurcation diagram for the original logistic map ($k = 0$) with control parameter μ in $[3.4, 4]$, and the corresponding bifurcation diagram for k_1 , k_2 and k_3 -logistic map. We also computed the firsts skeleton bifurcation curves [52] (see Fig. 3-b)) from the critical point $x_c = 0.5$ as a parameter of the function $P_n(\mu)$ given at Eq. 5, and detailed at the Appendix 8, which depicts the colored lines superimposed on the bifurcation diagram.

$$P_{n+1}(\mu) = \mu P_n(1 - P_n(\mu)), \quad (5)$$

where $P_0(\mu) = 0.5$. Moreover, we also plot the firsts skeleton bifurcation curves for the k_1 to k_3 -logistic map by extending the former equation and extracting the k -decimal digits using the Eq. 2 as follows

$$P_{n+1}^k(\mu) = \phi_{k,L}(P_n(\mu)). \quad (6)$$

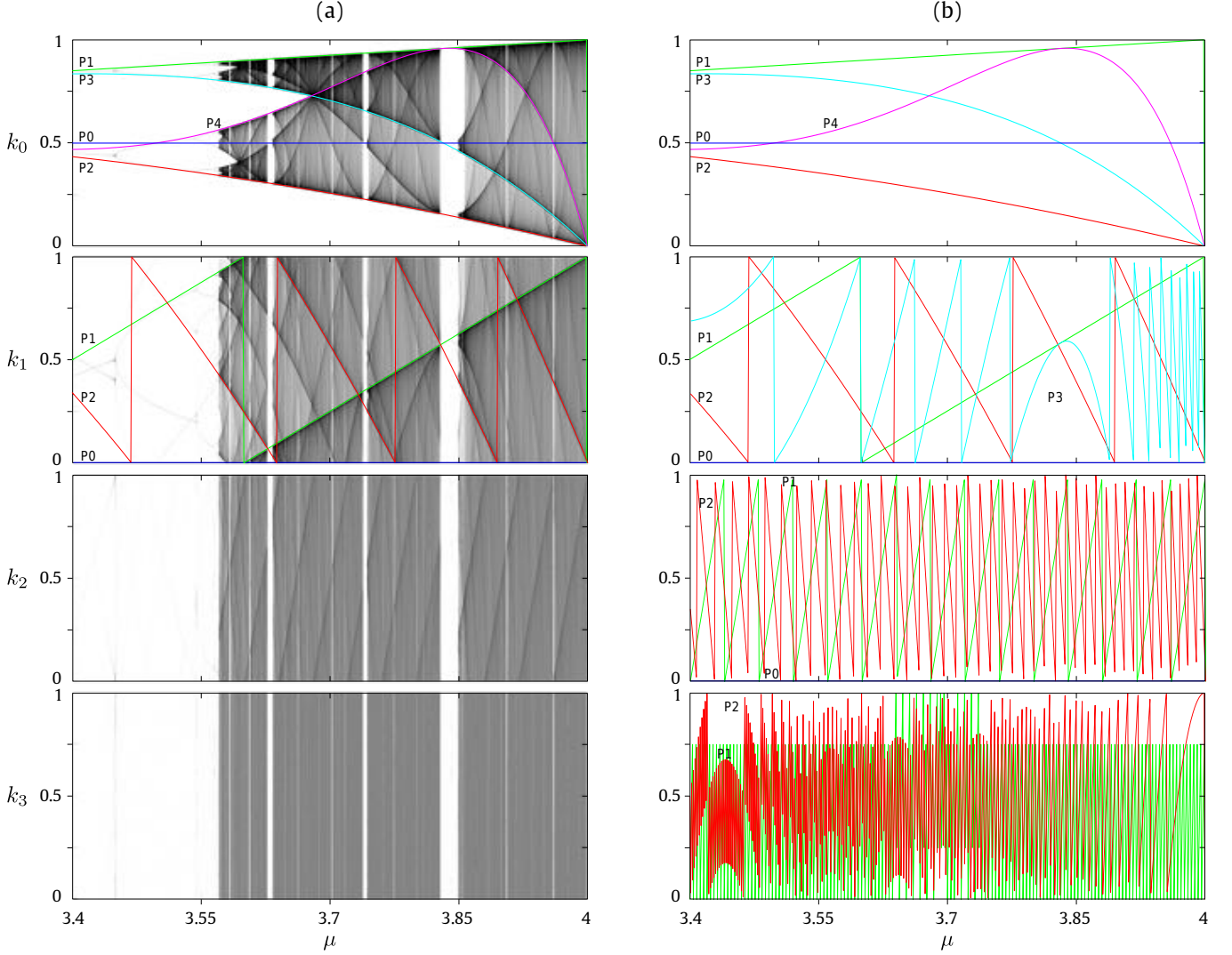


Figure 3: a) Bifurcation diagram of the k_0, k_1, k_2 and k_3 -logistic map (Eq. 2). The horizontal axis depicts $\mu \in [3.4, 4]$ (steps of 0.001). The vertical axis shows the possible long-term values of the corresponding k -logistic map, started from same initial condition, calculated over 10^5 iterations (first 200-th are the transient). b) The superimposed curves $P_n(\mu)$ (Eq. 6) correspond to the skeleton bifurcation (colored lines).

Here, we notice that the interspersed chaotic patterns nearly at the regions $\mu \in [3.57, 3.828]$ and $\mu \in [3.86, 4]$ get zigzagged (k_1), and starts to get gradually vanished (k_2) until become to seem random (k_3). Notwithstanding, the “islands of stability”, which can be easily visualized as the white strips of the bifurcation diagram (for instance intervals 3.4 to 3.57 and 3.828 to 3.86), remain constant for all the k -logistic map. Regarding the period-doubling bifurcation points, we can notice that their patterns become more filled as k increases. In some cases, the periodic regions, where the bifurcations intervals occur, are multiplied and the points are spread into the plot. Recalling that these phenomena was also observed at the time-evolution plot (see Fig. 2). The zigzagged behavior can also be noticed into the skeleton bifurcation (Fig. 3-b), since their curves get zigzagged (k_1 and k_2) and are saturated rapidly while k increases (k_3).

4.3 Lyapunov stability

Fig. 4 shows the approximated Lyapunov exponent (Eq. 4) of the k -logistic map orbits on the region $\mu \in [3.4, 4]$, which depicts the three types of dynamical behaviors, i.e. chaotic ($\lambda \geq 0$), periodic ($\lambda \approx 0$) and stable ($\lambda < 0$).

In the chaotic region $\mu \in [3.57, 3.828]$ and $\mu \in [3.86, 4]$, we can observe the positive LE curves of k_1 , k_2 and k_3 that are found nearly below to the LE $\lambda(\mu, k_0)$. In fact, we noticed an increment of the LE that obeys the upper bound found analytically at $\lambda = \ln 2 \approx 0.693$ for all of the LE curves $\lambda(\mu, x^k)$ obtained by using Eq. 4. On the other hand, in the non-chaotic regions, i.e. in the stable and periodic stability regions which includes the small gaps of the chaotic region (so called island of stability), we can observe a corresponding negative and zero LE curves for all of the $\lambda(\mu, x^k)$ curves. These results indicate that the orbits of the k -logistic are mandatory asymptotically stable or periodic in agreement to the behavior of the original orbit (k_0) as was previously shown in the bifurcation diagram and the time-evolution plot (see Fig. 2-3).

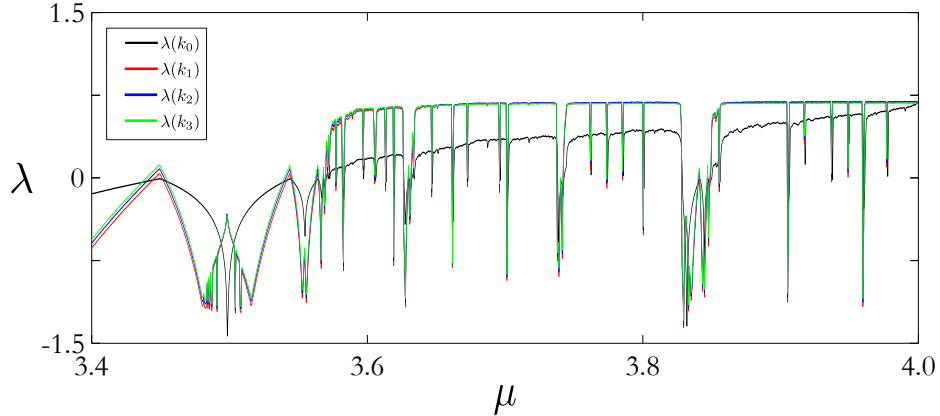


Figure 4: Lyapunov exponents of the k -logistic map for the $\lambda(k_0)$, $\lambda(k_1)$, $\lambda(k_2)$ and $\lambda(k_3)$. The horizontal axis depicts the LE in the region $\mu \in [3.4, 4]$ with steps of 0.0006. The LEs were computed using $T = 1000$ iterations and $\delta t = 50$ starting from $d_0 = 10^{-16}$.

4.4 Phase diagram

Another way to visualize the pseudo-randomness properties of the k -logistic map is by means of the phase diagram, or Poincaré diagram, that maps the value of x_{t+1}^k against x_t^k of a given orbit, or even three-dimensional by mapping x_{t+2}^k , x_{t+1}^k against x_t^k . For instance, Fig. 5 depicts the phase diagrams of the k -logistic map for four different orbits \mathcal{O}^k using $\mu = 4$ as a control parameter.

From top to down, the k_0 shows the classical inverted parabola with a maximum value at $x = 0.5$, whose pattern remain on the three-dimensional sketch. The row below shows the k_1 phase diagrams, here one can notice that the former parabola was transformed into a zigzagged pattern. The zigzagged patterns are progressively being spread and vanish into a random plot as can be observed from k_2 and k_4 . In fact, we can observe that the phase space is filled, i.e. the k -logistic map is producing almost all possible values, while k increases.

4.5 Frequency distributions

Fig. 6-a) depicts the frequency distribution curves for the orbits k_0 , k_1 , k_2 , and k_3 using parameter $\mu = 4$. Observing at the k_0 curve (gray), it depicts the well-known U pattern that follows the invariant probability density $\rho(x) = 1/\pi\sqrt{1-x^2}$ of the original logistic map [49]. Thus, it is noticed the presence of higher frequencies at the boundary regions $x \in [0, 0.1]$ and $x \in [0.9, 1]$ than at the center region.

Notwithstanding, at the inset plot of Fig. 6-a), we have noticed that the curves k_1 , k_2 and k_3 (colored) show a rapid decrease of the U pattern leading to a more uniform distribution as k is increased. The reader should notice that a plateau distribution is a expected for PRNG purposes. Moreover, this homogenization course is depicted in Fig. 6-b), which shows the difference Δ between the highest and lowest frequency obtained for k_0, k_1, \dots, k_{20} -logistic map, which is in agreement to the randomization course illustrated in the phase diagram at Fig. 5.

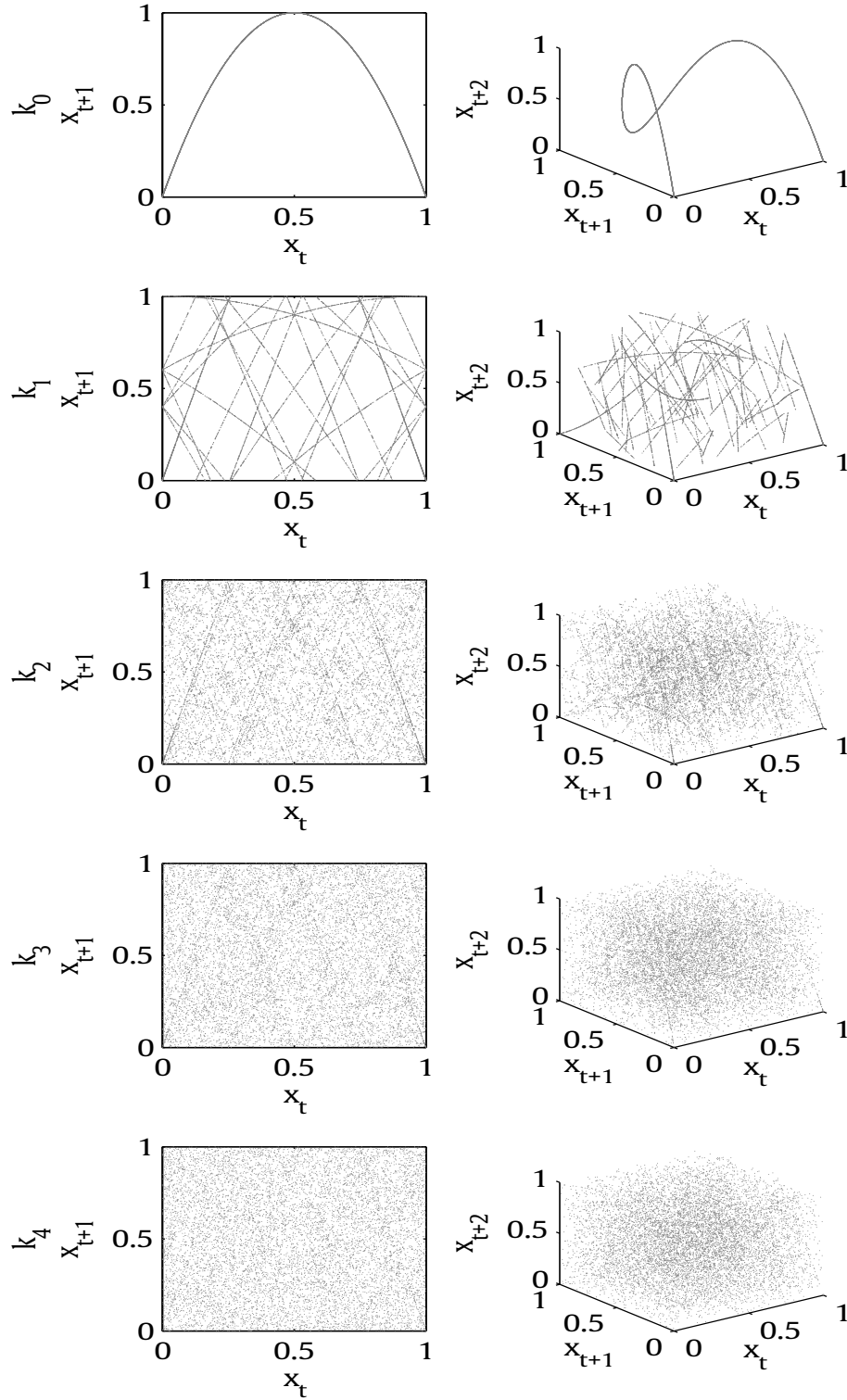


Figure 5: Phase diagrams for the k_0 , k_1 , k_2 , k_3 and k_4 -logistic map using $\mu = 4$. Two- and three-dimensional diagrams are shown on the left and right column, respectively. The horizontal and vertical axes show the phase space of x_t^k against x_{t+1}^k . Each orbit contains 10^4 points started from random initial conditions, where the first 200 iterations were discarded (transient time).

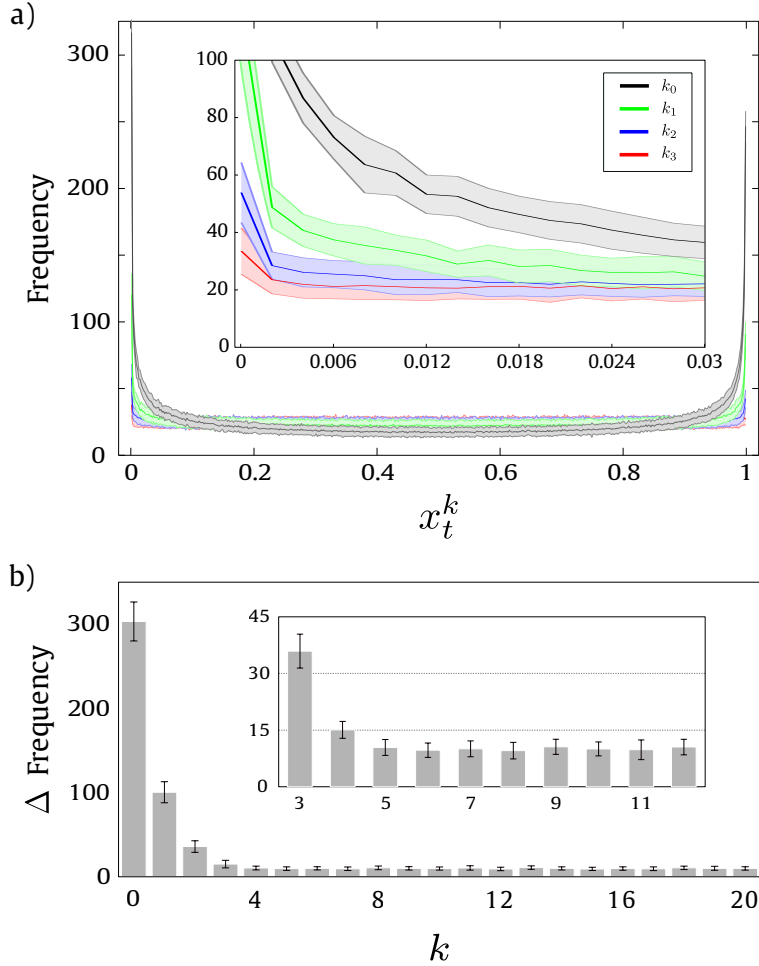


Figure 6: a) Frequency distribution curves for the k_0, k_1, k_2 and k_3 -logistic map using $L = 3$ and $\mu = 4$. Horizontal axis shows the $x \in [0, 1]$ (500 bins) and vertical axis shows the frequency of the 10^4 values discarding firsts 10^3 transient values. The curves represent the mean and standard deviation (shaded error bar) for sequences generated over 100 random initial conditions. The inset plot depicts a zoom on the windows $x \in [0, 0.03]$. b) Deviation between the highest and lowest value (Δ) obtained by the k_0, k_1, \dots, k_{20} -logistic map frequency distribution curve. The inner plot shows a magnification of the Δ frequency plot on the region k_3 to k_{11} .

5 PRNG based on k-logistic map

Before we introduce the PRNG based on the k -logistic map, we must constraint the Definition 2 given at Section 3. Therefore, the initial condition x_0 must be limited to $]0, 1[$. Additionally, the control parameter μ must be limited to the chaotic windows, e.g $\mu \in [3.57, 3.828]$ and $\mu \in [3.86, 4[$. These limitations must be considered in order to avoid, for instances, superstable points $f(\mu, 0) = f(\mu, 1) = 0$ and critical point $f(4, 0.5) = 1$, that lead to trivial values, and consequently, these are counterproductive for the generation of pseudo-random numbers. Yet, within the framework of PRNG purposes, we limited the PRNG based on k -logistic map by using the control parameter $\mu \rightarrow 4$ as a prototype for the chaotic regime, since it represents the maximum LE (Eq. 3), which has been conjectured by Collet&Eckman[53].

Therefore, in order to generate pseudo-random numbers using the k -logistic map, we simply discretized each x_t value in order to obtain a 32-bit integer as follows

$$\lfloor x_t^k (2^{32} - 1) \rfloor \quad (7)$$

Thus, in order to evaluate the inherent randomness properties of the chaotic dynamics of the k -logistic map, we subjected the orbits k_0, k_1, \dots, k_9 to two well-known pseudo-randomness suites namely Diehard [47] and NIST [48]. Both suits provide different tests based on hypothesis under p -values, where the null hypothesis H_0 determines

whether or not a specific binary sequence is accepted or rejected as random, otherwise is considered as failure. These battery tests are configured to read source file as a stream of bits, and therefore allowing to evaluate the randomness of the stream.

5.1 Diehard battery

The Diehard tests suite includes eighteen statistical tests (see more details in Ref. [47]). According to the Diehard documentation the binary sequences should be up to 10MBytes [47]. Therefore, we generated 100 files (each containing 12.5MBytes) for each orbit $\mathcal{O}^k(\mu, x_0)$, considering the chaotic region under $\mu \rightarrow 4$. Each sample file has been generated from a randomly chosen seed x_0 , and each value x_t^k was discretized as a 32-bit integer (Eq. 7), due to the Diehard restrictions [47].

Table 2: Average number of files that passed testes DIEHARD using k -logistic map PRNG (Eq. 7) from 100 files samples. Severe failed tests are shown in gray. All tests are passed at the interval $0.0001 < \text{p-value} < 0.9999$.

Diehard tests	k_0	k_1	k_2	k_3	k_4	k_5	k_6	k_7	k_8	k_9
BirthdaySpacings [KS]	100	100	100	100	100	100	100	100	100	100
OverlappingPermutations	99	97	98	95	98	96	98	98	99	100
Ranks31x31 matrices	100	100	100	100	100	100	100	100	100	100
Ranks32x32 matrices	100	100	100	100	100	100	100	100	100	100
Ranks6x8 matrices [KS]	0	0	25	99	100	100	100	100	100	100
Monkey20bitsWords [KS]	0	99	100	100	100	100	100	100	100	100
OPSO [KS]	98	99	100	100	100	100	100	100	100	100
OQSO [KS]	98	100	100	100	100	100	100	100	100	100
DNA [KS]	100	100	100	100	100	100	100	100	100	100
Count1sStream	0	0	0	98	100	100	100	100	100	100
Count1sSpecific [KS]	0	0	0	0	94	100	100	100	100	100
ParkingLot [KS]	100	100	100	100	100	100	100	100	100	100
MinimumDistance [KS]	96	100	100	100	100	100	100	100	99	100
RandomSpheres [KS]	100	100	100	100	100	100	100	100	100	100
Squeeze [KS]	100	100	100	100	100	100	100	100	100	100
OverlappingSums [KS]	100	100	100	100	100	100	100	100	100	100
Runs (up)	100	100	100	100	100	100	100	100	100	100
Runs (down)	100	100	100	100	100	100	100	100	100	100
Craps (wins)	100	100	100	100	100	100	100	100	100	100
Craps (throws/game)	100	100	100	100	100	100	100	100	100	100

The obtained number of files that passed the Diehard tests, i.e. $0.0001 < \text{p-value} < 0.9999$, are reported in Table 2. We observed that for certain tests (ranks6x8, monkey20bits, count1sStream and count1sSpecific) the k_0 to k_3 -logistic map have failed mandatory (shown in gray). Notwithstanding, most of the 100 files passed successfully when $k \geq 4$. Regarding the failed tests, for instance, the monkey20bits test treats sequences of bits as “words”, thus it counts the overlapping words in the stream looking for segments of 26-bits that do not appear from position 0 (leftmost) to 31. Therefore, as the logistic map from k_0 to k_3 maintains a probability distribution (U pattern), those values are not found in the stream, which influenced to fail the test.

5.2 NIST battery

The NIST test suite consists of fifteen statistical tests and the recommendations provided by the NIST [Special Publication 800-22 Revision 1a] were considered [48]. A binary sequence is considered succeed when the null hypothesis p -value ≥ 0.01 is accepted. Then, 10 files containing 100Mbits were generated based on the k -logistic map orbit $\mathcal{O}^k(\mu, x_0)$, where $\mu \rightarrow 4$ as control parameter. Thus, 10 samples containing binary sequences of length 10^6 bits were split from each file, being in total 100 samples.

The number of samples that passed the NIST battery, for each of the k -logistic map are reported in Table 3, for simplicity some of the sub-tests are not shown. Similar to the results obtained with the Diehard suit. We observed a partially failure to the NIST test when using k_0 , k_1 , and k_2 . More specifically, from top to down, i.e. runs, non-overlapping template, overlapping template, universal, approximate entropy and serial. Notwithstanding from $k \geq 3$, most of the 100 samples passed successfully.

Table 3: Number of files that passed the NIST test suits [48] for k -logistic map. Failed tests are shown in gray. All tests are passed at the $\alpha = 0.01$ significance level.

NIST tests	k_0	k_1	k_2	k_3	k_4	k_5	k_6	k_7	k_8	k_9
Frequency	98	99	99	99	99	99	99	99	99	99
BlockFrequency ($m = 128$)	0	1	66	95	98	98	99	100	99	99
CumulativeSums										
Forward sums	97	98	99	99	98	99	99	99	99	99
Reverse sums	97	99	99	99	99	99	99	99	99	99
Runs	0	0	14	91	98	99	99	99	99	100
LongestRun	0	0	15	89	98	99	98	100	99	99
Rank	99	100	99	99	99	99	99	99	99	99
FFT	77	98	99	99	99	99	99	99	99	99
Non-overlappingTemplate										
000000001	0	0	48	97	99	99	99	100	99	99
000000011	0	3	87	98	99	99	99	99	99	99
000000101	0	41	94	98	98	99	99	99	98	99
000000111	0	46	95	99	99	99	99	99	99	99
000001001	2	82	98	99	99	99	99	99	99	99
000001011	6	86	97	99	99	99	99	99	99	99
000001101	39	94	98	99	99	100	99	100	99	99
000001111	0	74	97	99	99	99	99	99	99	99
000010001	68	95	99	98	99	99	99	100	99	99
000010011	76	95	98	99	99	99	99	99	98	99
000010101	94	97	99	99	99	99	99	99	99	99
000010111	64	95	98	99	99	99	99	99	98	99
000011001	96	98	99	99	100	100	99	99	98	99
000011011	94	98	99	99	99	99	99	99	99	99
000011101	96	98	98	99	99	99	99	99	99	99
OverlappingTemplate	0	0	11	93	98	99	98	99	99	99
Universal	0	68	97	98	99	99	99	99	99	99
ApproxEntropy ($m = 10$)	0	0	64	98	99	99	99	100	99	99
RandomExcursions										
$x = -4$	90	98	99	99	98	99	99	99	99	100
$x = -3$	91	97	99	99	99	99	99	99	99	99
$x = -2$	94	99	98	99	99	98	99	99	99	99
$x = -1$	95	99	99	98	99	99	99	99	99	100
$x = 1$	95	99	99	99	99	99	99	99	98	100
$x = 2$	93	98	99	99	98	100	98	98	99	99
$x = 3$	89	97	98	99	99	99	98	98	99	99
$x = 4$	85	97	97	98	98	99	99	98	98	100
RandExcursVar										
$x = -9$	99	100	99	99	100	99	99	99	99	100
$x = -8$	99	99	99	99	99	99	99	99	99	100
$x = -7$	100	99	99	99	99	99	99	99	99	100
$x = -6$	100	99	99	99	99	99	98	99	99	99
$x = -5$	100	99	99	99	99	99	99	99	99	99
$x = -4$	99	100	99	99	99	99	99	99	99	99
$x = -3$	99	100	99	98	99	99	99	99	99	99
$x = -2$	99	99	99	98	99	99	99	100	99	99
$x = -1$	99	99	99	99	99	99	99	99	99	99
$x = 1$	100	100	99	100	100	99	99	99	99	99
$x = 2$	99	99	99	100	99	99	99	99	99	100
$x = 3$	99	99	98	99	99	99	99	99	99	100
$x = 4$	99	99	99	100	99	99	99	99	99	99
$x = 5$	99	99	98	100	98	99	98	99	99	99
$x = 6$	99	98	98	99	98	99	99	99	99	99
$x = 7$	99	98	99	100	98	100	99	99	99	99
$x = 8$	99	99	100	99	99	99	99	100	99	99
$x = 9$	99	98	100	99	98	99	99	100	99	99
Serial ($m = 16$)										
Serial 1	0	1	82	96	98	99	99	98	99	99
Serial 2	10	81	95	98	98	99	99	99	98	99
LinearComplexity ($M = 500$)	99	98	99	99	99	99	99	98	99	99

6 Extending to the k -tent map

Besides we have been focused extensively on the k -logistic map, our approach of the deep-zoom using the k -right digits can be extended to other chaotic maps in the unitary interval such as the tent map, which is given by Eq. 8.

$$x_{t+1} = f(\delta, x_t) = \begin{cases} \delta x_t, & \text{if } x_t < 0.5 \\ \delta(1 - x_t), & \text{if } x_t \geq 0.5, \end{cases} \quad (8)$$

where $x_t \in M = [0, 1]$ and $\delta \in U = [0, 2]$. Therefore, we extended the definitions given in Section 3. Thus, given an orbit of the original tent map $\mathcal{O}(\delta, x_0) = \{x_0, \dots, x_t\}$ and the resulting orbit $\mathcal{O}^k(\delta, x_0) = \{x_0^k, \dots, x_t^k\}$, from which we can use the generalized Eq. 2.

In a similar manner to the former experiments, here we also analyzed the overall dynamic properties of the k -tent map for PRNGs purposes. Thus, we also limited the experiments to the chaotic regime of the k -tent map by using the control parameter $\delta = 2$.

6.1 Bifurcation diagram of the k -tent map

Moreover, Fig. 7 shows the bifurcation and skeleton diagram for the k -tent map. We observed a similar phenomenon as reported on the k -logistic map (Fig. 3). Such that, as the k digits are increased, the orbits get twisted rapidly, the forks of the periods get stretched, while the steady regions remain. Moreover, the superimposed skeleton bifurcation also shown a zigzagged behavior which refers to a more irregular patterns.

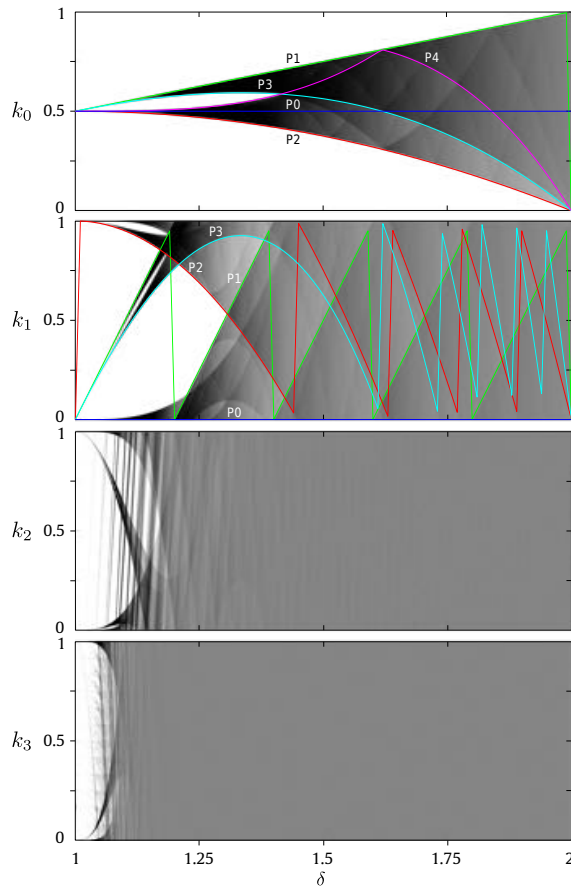


Figure 7: Bifurcation diagram of the k_0 , k_1 , k_2 and k_3 -tent map (Eq. 8). The horizontal axis shows $\mu \in [1, 2]$ (steps of 0.001), and the vertical axis depicts the long-term values of the k -tent map, started from same initial condition. We calculated over 10^5 iterations and discarding first 200 transient values. The superimposed curves $P_{n+1}(\delta)$ correspond to the skeleton bifurcation (dark lines) regarding the tent map, where $P_{n+1}(\delta) = f(P_n, \delta)$ with $x_c = 0.5$.

6.2 Phase diagram of the k -tent map

The phase diagrams of the k -tent map are shown in Fig. 8 (from top to down) corresponding to the k_0 to k_5 . We noticed that the k -tent map behaves similar to the logistic map (see Fig. 5) in terms of the randomization course as k is increased. Here, the characteristic tent pattern (k_0), from which it received its name, gets zigzagged (k_1), until it gets more diffused. Although some fuzzy patterns still remain at the three-dimensional phase diagram of k_4 . However, the phase-space begins to randomize from $k \geq 5$.

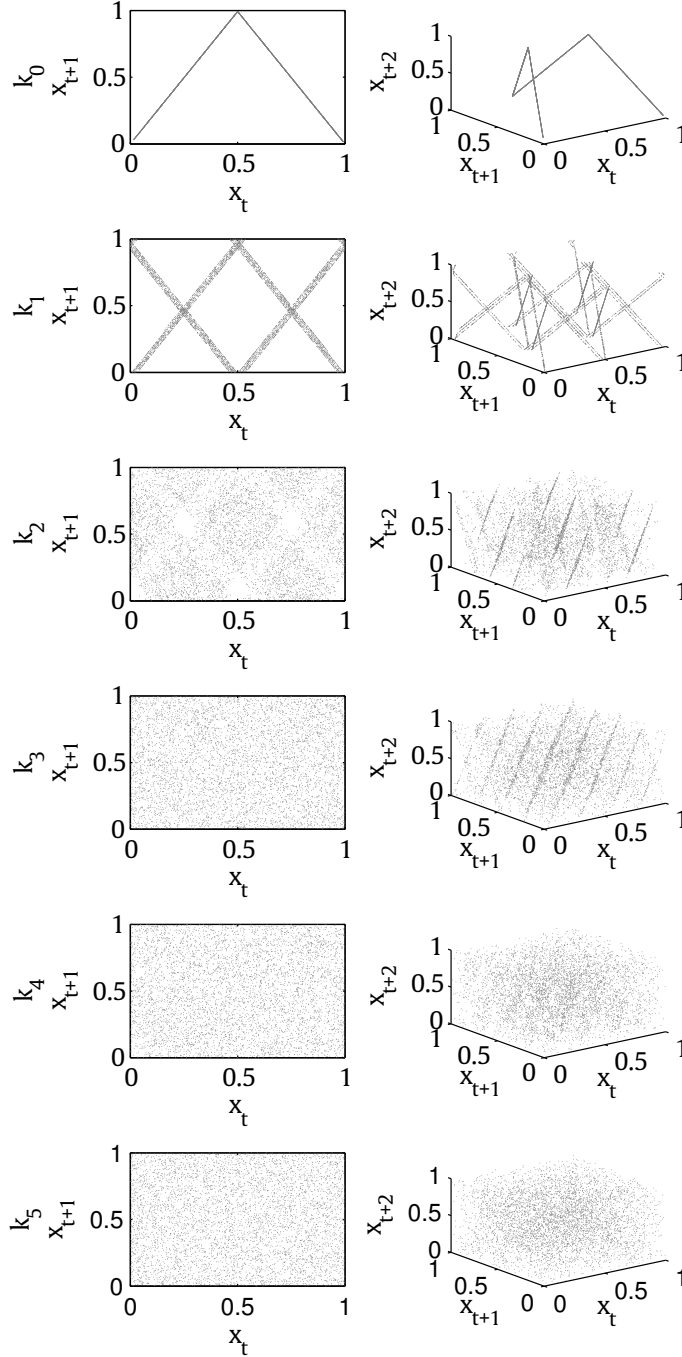


Figure 8: Phase diagrams for the k_0 , k_1 , k_2 , k_3 , k_4 and k_5 using $\delta = 2$. Two- and three-dimensional phase diagrams are shown on the left and right, respectively. The horizontal and vertical axes show the phase space of x_t against x_{t+1} and x_{t+2} . Each orbit contains 10^4 points from a random initial condition, the first 200 were discarded (transient period).

6.3 PRNG based on k -tent map

We also used the k -tent map for PRNG purposes. Similar to the k -logistic map, here we restricted the phase-space M to the interval $]0, 1[$ and the control parameter to the chaotic windows, e.g $\delta \rightarrow 2$. Thus, in order to generate numbers, we discretize the x_t^k values from the k -tent map into 32-bit integers as defined at Eq. 7. We setup the same configuration for the experiments using the Diehard [47] and NIST [48] suit tests. Table 6.3 and Table 5 reported the number of files that have passed the pseudo-randomness tests to both suits, respectively.

Regarding these tables, we observed a partially failure to the Diehard test from k_0 to k_5 -tent map. More precisely, the sub-tests Ranks6x8 matrices, OQSO, Count1sStream and Count 1s specifics. Notwithstanding from $k \geq 6$, most of the 100 samples passed successfully. In contrast to the k -logistic map, the k -tent map have passed successfully to the NIST suit for all of the k parameters.

Table 4: Average number of files that passed testes DIEHARD using k -tent map PRNG (Eq. 7) from 100 files samples. Severe failed tests are shown in gray. All tests are passed at the interval $0.0001 < p\text{-value} < 0.9999$.

Diehard tests	k_0	k_1	k_2	k_3	k_4	k_5	k_6	k_7	k_8	k_9
BirthdaySpacings [KS]	100	100	100	100	100	100	100	99	100	100
OverlappingPermutations	99	97	100	99	96	98	97	98	100	97
Ranks31x31 matrices	100	100	100	100	100	100	100	100	100	100
Ranks32x32 matrices	100	100	100	100	100	100	100	100	100	100
Ranks6x8 matrices [KS]	0	0	0	100	100	100	100	100	100	100
Monkey20bitsWords [KS]	100	100	100	100	100	100	100	100	100	100
OPSO [KS]	100	100	100	100	100	100	100	100	100	100
OQSO [KS]	0	0	0	100	100	100	100	100	100	100
DNA [KS]	100	100	100	100	100	100	100	100	100	100
Count1sStream	0	0	0	0	100	100	100	100	100	100
Count1sSpecific [KS]	0	0	0	0	0	0	100	100	100	100
ParkingLot [KS]	100	100	100	100	100	100	100	100	100	100
MinimumDistance [KS]	81	95	94	100	98	98	97	99	98	99
RandomSpheres [KS]	100	100	100	100	100	100	100	100	100	100
Squeeze [KS]	100	100	100	100	100	100	100	100	100	100
OverlappingSums [KS]	100	100	100	100	100	100	100	100	100	100
Runs (up)	100	100	100	100	100	100	100	100	100	100
Runs (down)	100	100	100	100	100	100	100	100	100	100
Craps (wins)	100	100	100	100	100	100	100	100	100	100
Craps (throws/game)	100	100	100	100	100	100	100	100	100	100

6.4 Comparison with other PRNGs

For performance comparison of the pseudo-randomness properties of the k -logistic map and the k -tent map with classical PRNGs, we have chosen most popular PRNGs, such as the congruential linear generator (LCG) [1, 2] and the Mersenne Twister (MT) [14]. The LCG is defined by the recurrence relation given by $x_{n+1} = (ax_n + c) \bmod m$, where the parameters a , c and m correspond to the integer parameters (the added, the constant, the multiplier) of the LCG generator. Here, we implemented the Java LCG version, using $a = 11$, $c = 25214903917$, $m = 2^{48}$. Furthermore, we used the Java version² of the original Mersenne Twister PRNG [14].

The average number of files that passed to the Diehard test is summarized in Table 6.4. This Table shows comparable results obtained for the LCG and the MT PRNGs with the k_4 -logistic map.

Moreover, Fig. 9 depicts the comparison of the average number of passed files from the Diehard suit of the k -logistic map, k -tent map from k_0 to k_{100} , LCG and MT generators. Therefore, based on the Student's t-test, we compare the means of all of the results from the Diehard test with a confidence level of 95%. We observe that the logistic map outperformed the tent map regarding the battery of pseudo-randomness tests. Moreover, observing at the inner plot on Fig. 9, when comparing our approach to the LCG and the MT PRNGs, we observed that from $k \geq 3$ the logistic map obtained superior pseudo-randomness properties than the LCG, while from $k \geq 3$ the logistic map performed just as well as the Mersenne Twister PRNG.

²Copyright (c) 2003 by Sean Luke <https://cs.gmu.edu/~sean/research/mersenne>

Table 5: Number of files that passed the NIST test suits [48] for k -tent map. All tests are passed at the $\alpha = 0.01$ significance level.

NIST tests	k_0	k_1	k_2	k_3	k_4	k_5	k_6	k_7	k_8	k_9
Frequency	98	99	99	99	99	99	98	99	99	99
BlockFrequency ($m = 128$)	100	99	99	100	99	100	99	100	99	99
CumulativeSums										
Forward sums	98	99	99	98	99	99	98	99	99	99
Reverse sums	98	99	99	99	99	99	99	99	99	99
Runs	79	92	98	99	99	99	99	99	99	99
LongestRun	97	99	99	99	99	99	99	99	99	99
Rank	99	99	99	99	99	99	99	99	100	99
FFT	99	99	99	99	99	99	99	99	98	99
Non-overlappingTemplate										
000000001	75	97	99	99	99	99	99	99	98	99
000000011	89	97	99	100	99	99	98	99	99	99
000000101	92	98	99	99	100	99	100	98	99	99
000000111	91	99	99	99	99	99	99	99	99	99
000001001	92	99	99	99	99	99	100	99	99	99
000001011	93	99	99	99	99	99	99	99	99	99
000001101	95	99	99	99	99	100	99	99	99	99
000001111	90	98	99	99	99	99	99	99	99	99
000010001	93	100	99	99	99	98	99	99	99	99
000010011	93	99	98	99	99	99	99	99	99	99
000010101	94	99	99	99	99	99	99	99	99	100
000010111	93	99	99	99	99	99	99	99	99	99
000011001	93	99	99	99	99	99	100	100	99	99
000011011	94	98	99	99	99	99	99	99	99	99
000011101	93	98	99	99	99	99	99	99	99	99
OverlappingTemplate	62	91	99	99	99	99	99	99	99	99
Universal	97	98	99	99	99	99	99	99	98	99
ApproxEntropy ($m = 10$)	82	99	99	99	99	99	99	99	99	99
RandomExcursions										
$x = -4$	98	99	99	98	99	100	98	98	99	99
$x = -3$	100	98	99	98	99	99	99	99	99	99
$x = -2$	98	99	99	99	99	99	99	99	100	99
$x = -1$	99	99	99	99	98	99	99	99	99	99
$x = 1$	99	99	99	99	99	98	100	99	99	99
$x = 2$	100	98	99	99	99	100	99	99	98	99
$x = 3$	99	99	99	99	99	100	99	99	99	99
$x = 4$	98	99	98	99	99	99	99	99	99	99
RandExcursVar										
$x = -9$	99	100	99	99	100	99	99	99	99	98
$x = -8$	99	99	99	100	100	99	100	99	99	98
$x = -7$	99	99	99	100	99	99	99	100	99	98
$x = -6$	99	99	100	100	100	99	99	99	98	99
$x = -5$	99	99	99	100	100	99	99	99	99	98
$x = -4$	99	99	99	99	99	99	99	99	100	99
$x = -3$	99	99	100	99	100	99	99	100	99	99
$x = -2$	99	99	100	100	99	99	100	99	99	99
$x = -1$	99	99	99	99	99	99	99	99	99	98
$x = 1$	99	99	98	99	99	99	98	100	98	99
$x = 2$	98	99	98	99	99	99	98	99	98	99
$x = 3$	98	99	99	99	99	100	98	99	99	99
$x = 4$	99	99	98	99	98	99	99	99	99	99
$x = 5$	98	99	98	99	98	99	98	99	99	99
$x = 6$	98	99	99	99	99	99	99	99	99	99
$x = 7$	99	100	100	99	99	99	98	99	99	99
$x = 8$	99	99	99	99	99	99	99	99	99	99
$x = 9$	99	99	99	99	99	99	98	99	99	99
Serial ($m = 16$)										
Serial 1	99	99	99	99	99	99	99	99	99	99
Serial 2	99	99	99	99	100	99	99	99	99	99
LinearComplexity ($M = 500$)	99	99	99	99	99	100	99	99	98	99

Table 6: Comparison of the avg. number of passed testes DIEHARD using the k_4 -logistic map PRNG and the congruential linear generator (LCG) and the Mersenne Twister PRNG (MT). Severe failed tests are shown in gray. All tests are passed at the interval $0.0001 < p\text{-value} < 0.9999$.

Diehard tests	logistic map (k_4)	LCG	MT
BirthdaySpacings [KS]	100	100	100
OverlappingPermutations	98	99	94
Ranks31x31 matrices	100	100	100
Ranks32x32 matrices	100	100	100
Ranks6x8 matrices [KS]	100	100	100
Monkey20bitsWords [KS]	100	100	100
OPSO [KS]	100	58	100
OQSO [KS]	100	0	100
DNA [KS]	100	0	100
Count1sStream	100	100	100
Count1sSpecific [KS]	94	100	100
ParkingLot [KS]	100	100	100
MinimumDistance [KS]	100	100	100
RandomSpheres [KS]	100	100	100
Squeeze [KS]	100	100	100
OverlappingSums [KS]	100	100	100
Runs (up)	100	100	100
Runs (down)	100	100	100
Craps (wins)	100	100	100
Craps (throws/game)	100	100	100

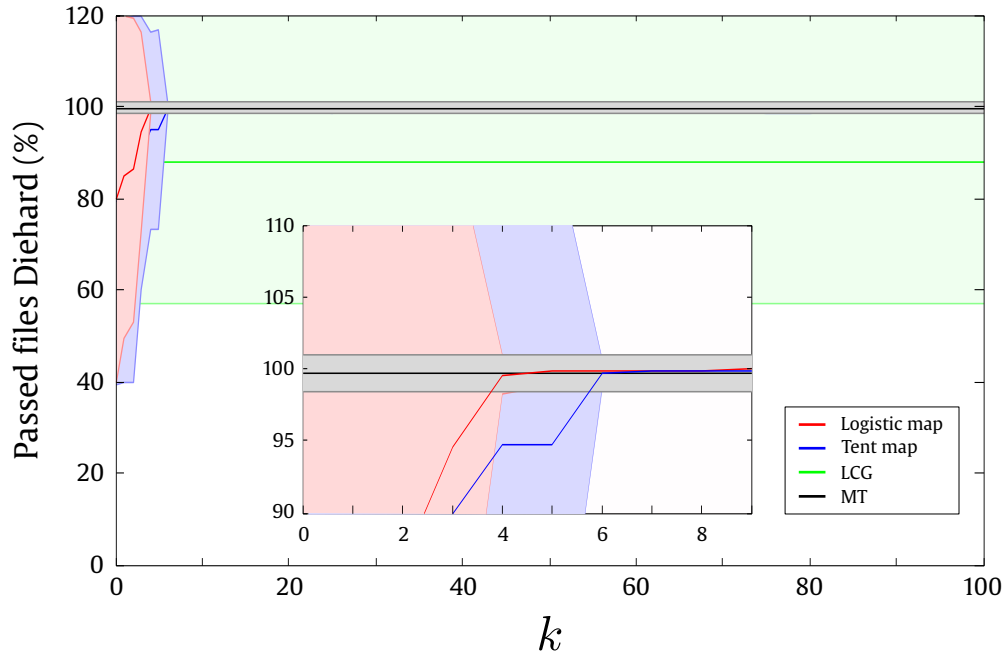


Figure 9: Average number of files that passed on the Diehard test of the k -logistic map, k -tent map for k_0 to k_{100} , linear congruential generator (LCG) and Mersenne Twister (MT) PRNGs. The vertical axis indicates the average number while the horizontal axis the different values of k -digits. The curves represents the mean and standard deviation (shaded error bar). The inner plot shows the zoom of the region between $k \in [0, 9]$.

7 Discussions

In this work, we have focused on the logistic map to analyze the properties that arises from the k -right digits zoom. It was selected, due to its simplicity and to be a well-known chaotic system. Therefore, we conducted two types of analysis: (i) to investigate the overall dynamic properties of the map and (ii) to assess the pseudo-randomness quality of the proposed PRNG by using both statistical tests, i.e. Diehard and NIST suits.

In the first part, we analyzed the time-evolution (Fig. 2), the bifurcation diagram (Fig. 3), the Lyapunov exponent (Fig. 4), the Poincaré diagram (Fig. 5) and the frequency distribution (Fig. 6).

The time-evolution analysis demonstrated that the k -logistic map keeps the overall dynamics of the original logistic map. Therefore, the chaotic, periodic and stable regions are preserved, independently of the parameter k . Indeed, what was changed was the number of iterations to stabilize the system. Thus, within the chaotic regions, the number of iterations before diverge decreases with k , yet within the stable regions, the number of iterations to converge to a fixed point and the cycle length of the periodic regions increases with k .

Furthermore, the analysis of the bifurcation diagram and the Poincaré diagram reveal a fast randomization behavior as k increases. We observed an intensification of the chaotic behavior, which was corroborated by the Lyapunov exponent, since all the chaotic regions tended to achieve the maximal LE upper bound. Regarding the frequency distribution analysis, we also observed a rapid randomization as k increases, since the U pattern achieved a plateau distribution, which in principle indicates that the k -orbits visit virtually every region of the phase-space. Within all of these analysis, we found that the pseudo-random properties of the k -logistic map can be noticeably improved as k is increased. In fact, the patterns become more and more diffused until becoming visually indistinguishable ($k \geq 4$).

In the second part of the experiments, regarding the pseudo-randomness tests, we found that the sequences generated when using the $k \geq 4$ -logistic map and $k \geq 5$ -tent map passed successfully to both the Diehard and NIST randomness tests.

8 Conclusions

In this paper, we proposed an approach to increase the pseudo-randomness properties of a chaos-based PRNG by means of a “deep-zoom” exploration. The main idea is to compound new values from the k -right digits, after the decimal separator, from the outcomes of the map, to then expand them to a larger number of pseudo random bits. The deep-zoom exploration was motivated by the facts that the chaotic systems rely analytically on the infinitesimal digits of precision, from which in principle, an infinite number of patterns can be extracted.

We proposed a general approach that can be directly applied to any one-dimensional chaotic map in the unit interval (i.e $x_t \in [0,1]$). Nevertheless, it can be adapted to other chaotic systems, that does not satisfy the former condition, such as the Hénon map, Gaussian map, Lorenz attractor, etc, through a proper adjustment of the scale of the phase-space, which implies to compound new values x_t^k into the same interval of the phase-space $M \in \mathbb{R}$.

Throughout this manuscript, we found that the pseudo-randomness properties of a chaotic map can be improved as k is increased, i.e a rapid transition from a “weak” to a “strong” randomness within the k -right sequences. Indeed, the overall dynamic analysis and the pseudo-randomness tests suggest that the quality performance of the proposed PRNG settle down in $k \geq 4$ and $k \geq 5$ for the logistic map and tent map, respectively.

Furthermore, we also observed that our proposed nonlinear PRNG can be compared to the popular Mersenne Twister PRNG in terms of pseudo-randomness quality provided by the statistical tests Diehard and NIST. Although, these qualifications should not be considered as an ultimate indicator, but rather as a detector of deviations from randomness. Since, these tests are supported statistically on pass and fail values instead of numerical values that may lead to a measure from a weakness to a strength quality. Therefore, there is still a lack of methods that shows a measurement of a PRNG quality in terms of pseudo-randomness tests.

Moreover, the PRNG requirements were accomplished, since we met an uniform distribution, long periodicity, indistinguishable statistical patterns. In fact, the proposed PRNG base on the deep zoom of chaotic maps can be a good candidate for potential applications such as simulations, computer games, programming language, cryptography, among others.

Finally, in this manuscript we showed that our approach applied to a simple chaotic map are able to produce pseudo-random numbers of high-quality by taking advantages from their deep-zoom properties.

Acknowledgements

J.M. acknowledges a scholarship from the Brazilian agency CAPES (PROEX). O.M.B. acknowledges support from CNPq (Grants #307797/2014-7 and #484312/2013-8) and FAPESP (Grant #14/08026-1).

References

- [1] Donald E. Knuth. *The Art of Computer Programming, Volume 2 (3rd Ed.): Seminumerical Algorithms*. Addison Wesley Longman Publishing Co., Inc., Boston, MA, USA, 1997.
- [2] William H. Press, Brian P. Flannery, Saul A. Teukolsky, and William T. Vetterling. *Numerical recipes in C: The art of scientific computing*. Fortran numerical recipes. Cambridge University Press, Cambridge, UK, 2 edition, 1992.
- [3] Nicholas Metropolis and Stanislaw M. Ulam. The Monte Carlo method. *Journal of the American Statistical Association*, 44(247):335–341, 1949.
- [4] M.P. Silverman, Wayne Strange, Chris R. Silverman, and T.C. Lipscombe. Tests of alpha-, beta-, and electron capture decays for randomness. *Physics Letters A*, 262(4–5):265–273, 1999.
- [5] John Walker. HotBits: Genuine random numbers, generated by radioactive decay, 2006.
- [6] Marco Bucci, Raimondo Luzzi, Lucia Germani, Alessandro Trifiletti, and Mario Varanonuovo. A high-speed oscillator-based truly random number source for cryptographic applications on a smart card IC. *IEEE Transactions on Computers*, 52:403–409, 2003.
- [7] W. T. Holman, J. A. Connelly, and A. B. Dowlatabadi. An integrated analog/digital random noise source. *IEEE Transactions on Circuits and Systems I: Fundamental Theory and Applications*, 44(6):521–528, 1997.
- [8] Mads Haahr. random.org: Introduction to randomness and random numbers, 1999.
- [9] L.C. Noll, R.G. Mende, and S. Sisodiya. Method for seeding a pseudo-random number generator with a cryptographic hash of a digitization of a chaotic system, 1998. US Patent 5,732,138.
- [10] Min Ren, E Wu, Yan Liang, Yi Jian, Guang Wu, and Heping Zeng. Quantum random-number generator based on a photon-number-resolving detector. *Phys. Rev. A*, 83:023820, 2011.
- [11] Feihu Xu, Bing Qi, Xiongfeng Ma, He Xu, Haoxuan Zheng, and Hoi-Kwong Lo. Ultrafast quantum random number generation based on quantum phase fluctuations. *Opt. Express*, 20(11):12366–12377, 2012.
- [12] ID Quantique SA. Random number generation using quantum physics. Version 3.0, 2010.
- [13] Persi Diaconis, Susan Holmes, and Richard Montgomery. Dynamical bias in the coin toss. *SIAM Rev.*, 49(2):211–235, 2007.
- [14] Makato Matsumoto and Takuji Nishimura. Mersenne Twister: A 623-Dimensionally Equidistributed Uniform Pseudo-Random Number Generator. *ACM Transactions on Modeling and Computer Simulation*, 8:3–30, 1998.
- [15] Jürgen Eichenauer and Jürgen Lehn. A non-linear congruential pseudo random number generator. *Statistische Hefte*, 27(1):315–326, 1986.
- [16] A. Peinado and A. Fúster-Sabater. Generation of pseudorandom binary sequences by means of linear feedback shift registers (LFSRs) with dynamic feedback. *Mathematical and Computer Modelling*, 57(11-12):2596–2604, 2013.
- [17] G. Markowsky. The sad history of random bits. *Journal of Cyber Security and Mobility*, 3:1–24, 2014.
- [18] A. Hodges. *Alan Turing: The Enigma*. Walker & Company, 2000.
- [19] L. Kocarev. Chaos-based cryptography: a brief overview. *IEEE Circuits and Systems Magazine*, 1(3):6–21, 2001.

- [20] Vinod Patidar, K. K. Sud, and N. K. Pareek. A pseudo random bit generator based on chaotic logistic map and its statistical testing. *Informatika (slovenia)*, 33:441–452, 2009.
- [21] M. Baptista. Cryptography with chaos. *Phys Lett A*, 240:50–54, 1998.
- [22] Stephen Wolfram. Cryptography with cellular automata. In *Lecture Notes in Computer Sciences; 218 on Advances in cryptology—CRYPTO 85*, pages 429–432, New York, NY, USA, 1986. Springer-Verlag New York, Inc.
- [23] Gonzalo Álvarez and Shujun Li. Some basic cryptographic requirements for chaos-based cryptosystems. *International Journal of Bifurcation and Chaos*, 16:2129–2151, 2006.
- [24] Jeaneth Machicao, Jan M Baetens, Anderson G Marco, Bernard De Baets, and Odemir M Bruno. A dynamical systems approach to the discrimination of the modes of operation of cryptographic systems. *Communications in Nonlinear Science and Numerical Simulation*, 29(1-3):102–115, 2015.
- [25] David Arroyo. *Framework for the analysis and design of encryption strategies based on discrete-time chaotic dynamical systems*. PhD thesis, Universidad Politécnica de Madrid, Madrid, 2009.
- [26] Anderson Marco, Alexandre Souto Martinez, and Odemir Martinez Bruno. Fast, Parallel and Secure Cryptography Algorithm Using Lorenz’s attractor. *International Journal of Modern Physics C*, 21(03):365, 2010.
- [27] Liu Nian-sheng. Pseudo-randomness and complexity of binary sequences generated by the chaotic system. *Communications in Nonlinear Science and Numerical Simulation*, 16(2):761–768, 2011.
- [28] P. Dabal and R. Pelka. A chaos-based pseudo-random bit generator implemented in FPGA device. In *Design and Diagnostics of Electronic Circuits Systems (DDECS), 2011 IEEE 14th International Symposium on*, pages 151–154, 2011.
- [29] S. Behnia, A. Akhavan, A. Akhshani, and A. Samsudin. A novel dynamic model of pseudo random number generator. *Journal of Computational and Applied Mathematics*, 235(12):3455 – 3463, 2011.
- [30] L. Min, K. Hu, L. Zhang, and Y. Zhang. Study on pseudorandomness of some pseudorandom number generators with application. In *Computational Intelligence and Security (CIS), 2013 9th International Conference on*, pages 569–574, 2013.
- [31] HanPing Hu, LingFeng Liu, and NaiDa Ding. Pseudorandom sequence generator based on the chen chaotic system. *Computer Physics Communications*, 184(3):765–768, 2013.
- [32] Lequan Min, Tianyu Chen, and Hongyan Zang. Analysis of fips 140-2 test and chaos-based pseudorandom number generator. *Chaotic Modeling and Simulation*, 2(1):273–280, 2013.
- [33] M. Franois, T. Grosgees, D. Barchiesi, and R. Erra. Pseudo-random number generator based on mixing of three chaotic maps. *Communications in Nonlinear Science and Numerical Simulation*, 19(4):887–895, 2014.
- [34] İsmail Öztürk and Recai Kılıç. A novel method for producing pseudo random numbers from differential equation-based chaotic systems. *Nonlinear Dynamics*, 80(3):1147–1157, 2015.
- [35] M. Tomassini, M. Sipper, and M. Perrenoud. On the generation of high-quality random numbers by two-dimensional cellular automata. *IEEE Transactions on Computers*, 49(10):1146–1151, 2000.
- [36] J. Machicao, A. Marco, and O. M. Bruno. Chaotic encryption method based on life-like cellular automata. *Expert Systems with Applications*, 39:12626–12635, 2012.
- [37] Jason Spencer. Pseudorandom bit generators from enhanced cellular automata. *J. Cellular Automata*, 10(3–4):295–317, 2015.
- [38] A. Akhshani, A. Akhavan, S.-C. Lim, and Z. Hassan. An image encryption scheme based on quantum logistic map. *Communications in Nonlinear Science and Numerical Simulation*, 17(12):4653–4661, 2012.
- [39] A. Akhshani, A. Akhavan, A. Mobaraki, S.-C. Lim, and Z. Hassan. Pseudo random number generator based on quantum chaotic map. *Communications in Nonlinear Science and Numerical Simulation*, 19(1):101–111, 2014.

- [40] Y-G Yang and Q-Q Zhao. Novel pseudo-random number generator based on quantum random walks. *Scientific Reports*, 6:20362, 2016.
- [41] A. Uchida, K. Amano, M. Inoue, K. Hirano, S. Naito, H. Someya, I. Oowada, T. Kurashige, M. Shiki, S. Yoshimori, K. Yoshimura, and P. Davis. Fast physical random bit generation with chaotic semiconductor lasers. *Nat. Photonics*, 2(12):728–732, 2008.
- [42] Ido Kanter, Yaara Aviad, Igor Reidler, Elad Cohen, and Michael Rosenbluh. An optical ultrafast random bit generator. *Nature Photon*, 4:58–61, 2010.
- [43] Gonzalo Álvarez, F. Montoya, M. Romera, and G. Pastor. Cryptanalysis of an ergodic chaotic cipher. *Physics Letters A*, 311(2–3):172–179, 2003.
- [44] K.J. Persohn and R.J. Povinelli. Analyzing logistic map pseudorandom number generators for periodicity induced by finite precision floating-point representation. *Chaos, Solitons & Fractals*, 45:238–245, 2012.
- [45] Hanping Hu, Yashuang Deng, and Lingfeng Liu. Counteracting the dynamical degradation of digital chaos via hybrid control. *Communications in Nonlinear Science and Numerical Simulation*, 19(6):1970 – 1984, 2014.
- [46] B.B. Mandelbrot. *The Fractal Geometry of Nature*. Henry Holt and Company, 1982.
- [47] G. Marsaglia. The Marsaglia random number CDROM, with the DIEHARD battery of tests of randomness, 1998.
- [48] Andrew Rukhin, Juan Soto, James Nechvatal, Miles Smid, Elaine Barker, Stefan Leigh, Mark Levenson, Mark Vangel, David Banks, and Alan Heckert. NIST Special Publication 800-22: A statistical test suite for random number generator for cryptographic applications. Technical report, National Institute of Standards and Technology, Gaithersburg, MD, USA, 2001.
- [49] E. Ott. *Chaos in Dynamical Systems*. Cambridge University Press, 2002.
- [50] Shujun Li, Qi Li, Wenmin Li, Xuanqin Mou, and Yuanlong Cai. *Statistical Properties of Digital Piecewise Linear Chaotic Maps and Their Roles in Cryptography and Pseudo-Random Coding*, pages 205–221. Springer Berlin Heidelberg, Berlin, Heidelberg, 2001.
- [51] Alan Wolf, Jack B Swift, Harry L Swinney, and John A Vastano. Determining lyapunov exponents from a time series. *Physica D: Nonlinear Phenomena*, 16(3):285–317, 1985.
- [52] Bai-Lin Hao. *Elementary symbolic dynamics and chaos in dissipative systems*. Singapore Teaneck, N.J. World Scientific, 1989.
- [53] P. Collet and J.P. Eckmann. *Iterated Maps on the Interval as Dynamical Systems*. Modern Birkhäuser Classics. Birkhäuser Boston, 2009.

Appendix A: Skeleton bifurcation

Bai-lin [52] introduced a family of recursive functions $\{P_n(\mu)\}$, where $n = 0, 1, \dots$, which correspond to the skeleton curves from a discrete dynamical system shown in a bifurcation diagram. The skeleton curves correspond to the characteristic dark lines and boundary zones as seen in the bifurcation diagrams shown in the logistic map (Fig. 3) and the tent map (Fig. 7). Here, we have shown the means to achieve the equation given at Eq. 5 as follows:

Definition 4. Considering that a DDS may have one or more critical point x_{c_i} , i.e. where its first derivative vanishes, i.e., $f'(\mu, x_{c_i}) = 0$, then it is obtained several sets of composite functions $\{P_n^i\}$, where the superscript i indicates the related point. Thus, starting from one critical point x_c , it is defined recursively on the form $P_{n+1} = f(\mu, P_n(\mu))$. Regarding the logistic map given its unique critical point $x_c = 0.5$, since its first derivative $f'(\mu, x_c) = \mu - 2\mu x = 0$, then the function P_n are polynomials of μ such as:

$$\begin{aligned}
 P_0(\mu) &= x_c \\
 P_1(\mu) &= \mu/4 \\
 P_2(\mu) &= 4\mu^2 - \mu^3/16 \\
 P_3(\mu) &= (\mu^3 - \mu^4)(\mu^3 - 4\mu^2 + 16)/256 \\
 P_4(\mu) &= (4\mu^4 - \mu^5)(\mu^3 - 4\mu^2 + 16) \\
 &\quad (\mu^7 - 8\mu^6 + 16\mu^5 + 16\mu^4 - 64\mu^3 + 256)/65536
 \end{aligned}$$

Furthermore, regarding the tent map and its unique critical point $x_c = 0.5$, the polynomials $P_n(\delta)$ are as follows:

$$\begin{aligned}
 P_0(\delta) &= x_c \\
 P_1(\delta) &= \delta/2 \\
 P_2(\delta) &= \begin{cases} \delta^2/2, & \text{for } \delta < 1 \\ \delta(1 - \delta)/2, & \text{for } \delta \geq 1 \end{cases}
 \end{aligned}$$